APS physics

CHORUS

This is the accepted manuscript made available via CHORUS. The article has been published as:

Photovoltaic anomalous Hall effect in line-node semimetals

Katsuhisa Taguchi, Dong-Hui Xu, Ai Yamakage, and K. T. Law

Phys. Rev. B **94**, 155206 — Published 28 October 2016

DOI: 10.1103/PhysRevB.94.155206

Photovoltaic anomalous Hall effect in line-node semimetals

Katsuhisa Taguchi,[1] Dong-Hui Xu,[2] Ai Yamakage,[1,3] and K. T. Law[2]

[1] *Department of Applied Physics, Nagoya University, Nagoya, 464-8603, Japan*
[2] *Department of Physics, Hong Kong University of Science and Technology, Clear Water Bay, Hong Kong, China*
[3] *Institute for Advanced Research, Nagoya University, Nagoya, 464-8601, Japan*

We theoretically study the circularly polarized light-induced Floquet state in line-node semimetals with time-reversal symmetry and inversion symmetry. It is found that the Floquet state can show the photovoltaic anomalous Hall effect when an applied circularly polarized light creates a gap the line node in the bulk and leaves Weyl point nodes. The Hall conductivity is sensitive to the location of the Fermi level: When the Fermi level is located at the node, the Hall conductivity depends on the radius of the line node and is nearly independent of the intensity of the light. Far from the line node, the Hall conductivity is dependent on the intensity of the light. The sensitive Fermi-level dependence of the Hall conductivity in the presence of a laser of weak intensity can have applications in phototransistors based on thin films of line-node semimetals.

I. INTRODUCTION

Topological matter has attracted enormous attention in recent years because it can host exotic edge or surface states protected by nontrivial bulk topologies. Topological insulators, which are well known examples, are characterized by a fully insulating gap in the bulk and symmetry-protected metallic states at the boundaries[1,2]. Currently, research interest in topological materials has shifted from insulators to semimetals, as semimetals with topologically non-trivial Fermi surfaces can also support robust surface states. In general, the bulk band structures of topological semimetals possess point or line nodes in the momentum space[3,4]. 3D Dirac semimetals form one class of topological semimetals with four-fold degenerate point nodes, where the electrons have linear dispersions near the Dirac nodes. Na_3Bi[5] and Cd_3As_2[6,7] have been experimentally confirmed to be topological Dirac semimetals, where the Dirac nodes are protected by a crystalline symmetry. If inversion or time-reversal symmetry is broken, each Dirac node splits into two Weyl nodes that are separated in the momentum space, and the systems become Weyl semimetals[8]. Weyl nodes with distinct chiralities lead to a variety of exotic measurable consequences such as Fermi arc surface states and chiral anomalies. Weyl semimetals have become a hot topic because real Weyl semimetal materials have been theoretically proposed[9,10] and experimentally discovered in inversion-symmetry-breaking TaAs-class crystals[11–14].

Unlike Dirac/Weyl semimetals, in which the conduction band touches the valence band at discrete points in the momentum space, the conduction and valence bands in topological line-node semimetals touch each other on closed lines, and symmetry protected drumhead surface states emerge[3,4,15–17]. Recently, several theoretical proposals[18–27] and experimental studies[26–32] on line-node materials have appeared. Because the dimension of line nodes is different from that of point nodes in Dirac/Weyl semimetals, we expect that line-node semimetals will exhibit new topological transport and response phenomena characteristics for line nodes. Several studies have shown novel phenomena in line-node semimetals, e.g., minimal conductivity[3,25], quantized Hall conductivity[25], a flat Landau level[33], plasmons[34,35], and electric polarization and orbital magnetization[36]. One method for realizing nontrivial transport phenomena in semimetals is to irradiate the materials using light. Dirac/Weyl semimetals in the presence of circularly polarized light have been theoretically studied within the framework of Floquet theory[37–39]. The circularly polarized light couples to electrons in a nontrivial way: the angular momentum of the incident light interacts with that of electrons, which can break the time-reversal symmetry. The anomalous Hall effect due to the light-induced interaction, which is called the photovoltaic anomalous Hall effect[40], occurs when the Fermi level is located near the Weyl nodes.

In this paper, we study the transport phenomena of line-node semimetals in the presence of circularly polarized light within the framework of Floquet theory. We find that the light-induced interaction in line-node semimetals, unlike that in Dirac/Weyl semimetals[37–39], has a strong dependence on the direction of incident light and is highly anisotropic. We show that photovoltaic anomalous Hall effect in line-node semimetals with time reversal and inversion symmetries, such as that in Ca_3P_2[28], can be generated by applying circularly polarized light. We calculate the Hall conductivity $\sigma_{zx}^{\mathrm{AHE}}(\epsilon_{\mathrm{F}})$ as a function of Fermi level ϵ_{F} and temperature. We find that for $\epsilon_{\mathrm{F}} = 0$, which means that the Fermi level is located at the line node, the Hall conductivity depends on the radius of the line-node, but that it does not depend on the strength of the light-induced interaction. For $\epsilon_{\mathrm{F}} \neq 0$, on the other hand, the Hall conductivity depends on both the radius of the line-node and the strength of light-induced interaction. As a result, the magnitude of $\sigma_{zx}^{\mathrm{AHE}}(\epsilon_{\mathrm{F}})$ is sensitive to ϵ_{F} in the presence of weak-intensity incident light.

II. MODEL

We consider a line-node semimetal with time-reversal and spatial-inversion symmetries that can be described

by a minimal two-band model. In the absence of an applied electromagnetic field, the low-energy effective model Hamiltonian of line node semimetal is expressed by[20,21,41]

$$H_0 = \sum_{\boldsymbol{k}} \psi^\dagger_{\boldsymbol{k}} \mathcal{H}_0 \psi_{\boldsymbol{k}}, \tag{1}$$

$$\mathcal{H}_0(\boldsymbol{k}) = \left(\frac{\hbar^2 k^2}{2m} - m_0\right)\tau^z s^0 + v k_z \tau^y s^0 - \epsilon_{\rm F}\tau^0 s^0, \tag{2}$$

where m is the effective mass of the electron; $\psi_{\boldsymbol{k}} = (\psi_{\uparrow,+}\ \psi_{\uparrow,-}\ \psi_{\downarrow,+}\ \psi_{\downarrow,-})^T$ is the annihilation operator with spin up ($\uparrow$), down ($\downarrow$), even- ($+$), and odd- ($-$) parity orbitals under the mirror reflection with respect to the $z=0$ plane; and $k^2 = k_x^2 + k_y^2 + k_z^2$ holds. $s^{x,y,z}$ ($\tau^{x,y,z}$) and s^0 (τ^0) are the Pauli matrices and the identity matrix in the spin (orbital) space, respectively. When the bands are inverted ($m_0 > 0$), a line node appears on the circle of $k_x^2 + k_y^2 = 2mm_0/\hbar^2$ and $k_z = 0$. m_0 and v are parameters corresponding to the radius of the line node and the velocity in the z direction, respectively.

Additionally, we take the electromagnetic fields for line-node semimetals into account. The total Hamiltonian is obtained using the Peierls substitution, i.e., $\boldsymbol{k} \to \boldsymbol{k} - e\boldsymbol{A}/\hbar$. Keeping the first-order term expansion about the vector potential $\mathbf{A}$, the total Hamiltonian is approximated by

$$H = H_0 + H_{\rm em}, \tag{3}$$

$$H_{\rm em} = -\sum_{\boldsymbol{k}} \psi^\dagger_{\boldsymbol{k}} \boldsymbol{j}\cdot\boldsymbol{A}\psi_{\boldsymbol{k}}. \tag{4}$$

where the charge current $\boldsymbol{j}$ is represented by

$$\boldsymbol{j} = \frac{e\hbar}{m}\left(\boldsymbol{k} - \frac{e}{2\hbar}\boldsymbol{A}\right)\tau^z s^0 - \frac{ev}{\hbar}\tau^y s^0 \boldsymbol{e}_z, \tag{5}$$

where $e < 0$ is the elementary charge of an electron and $\boldsymbol{e}_z$ is the unit vector along the z direction. The electric field $\boldsymbol{E}$ is obtained from the spatially-uniform vector potential $\boldsymbol{A}$; $\boldsymbol{E} = -\partial_t \boldsymbol{A}$.

In Sec. III, we note that $\boldsymbol{A} = \boldsymbol{A}_{\rm L}(t)$ and $\boldsymbol{E} = \boldsymbol{E}_{\rm L}$ denote the vector potential and electric field of the incident light, respectively. In Sec. IV, to consider the anomalous Hall effect, a DC electric field ($\boldsymbol{E}_{\rm dc}$) is also included: $\boldsymbol{E} \equiv \boldsymbol{E}_{\rm L} + \boldsymbol{E}_{\rm dc}$ and $\boldsymbol{A} \equiv \boldsymbol{A}_{\rm L} + \boldsymbol{A}_{\rm dc}$.

III. FLOQUET STATES

Based on the model Hamiltonian of Eqs. (1)-(4), we consider the Floquet state in line-node semimetals using the standard approach[37–40]. Consider the time-dependent vector potential $\mathbf{A}(t)$, which is a periodic function with a period of $2\pi/\Omega$. Then, the total Hamiltonian Eq. (3) is also periodic, as $\mathcal{H}(t) = \mathcal{H}(t + 2\pi/\Omega)$, with a frequency of incident light of Ω. Below, $\boldsymbol{A}_{\rm L}$ is assumed to be the monochromatic frequency of the coherent light. Then, the wave function of the Schrödinger equation $i\partial_t\psi(t) = H\psi(t)$ is given by $\psi(t) = \sum_u \phi_u e^{-i(\epsilon/\hbar + u\hbar\Omega)t}$, where ϵ is the Floquet quasi-energy and u takes all integer values. From the Schrödinger equation and the Floquet equation, $\sum_n \mathcal{H}_{u,n}\phi_n = (\epsilon + u\hbar\Omega)\phi_u$ is obtained. Here, $\mathcal{H}_{u,n} \equiv \frac{1}{\Omega/(2\pi)}\int_0^{\Omega/(2\pi)} \mathcal{H}(t) e^{i(u-n)\Omega t} dt + u\hbar\Omega\delta_{un}$ is the block Hamiltonian in the Floquet state. Using Eq. (1), the diagonal term becomes $\mathcal{H}_{u,u} = u\hbar\Omega + \frac{1}{\Omega/(2\pi)}\int_0^{\Omega/(2\pi)}\mathcal{H}(t)dt = u\hbar\Omega + \mathcal{H}_0 + \frac{e^2}{2m}|A_{\rm L}|^2\tau^z s^0$; the off-diagonal terms are $\mathcal{H}_{u,u+1} = \mathcal{H}^\dagger_{u+1,u} = -\frac{1}{\Omega/(2\pi)}\int_0^{\Omega/(2\pi)} \boldsymbol{j}\cdot\boldsymbol{A}_{\rm L}(t) e^{-i\Omega t} dt$. The other off-diagonal terms are identically zero. Each solution to the Floquet equation is regarded as a periodic steady state.

Next, we focus on the effective Hamiltonian $\tilde{\mathcal{H}}_{0,0}$, integrating out the higher-energy states $\phi_{n\geq 1}$. $H_{\rm em}$ renormalizes the parameters and introduces new terms into $\tilde{\mathcal{H}}_{0,0}$. Using the symmetry considerations, we find that $k_y\tau^x s^0$ (or $k_x\tau^x s^0$) is the only time-reversal-symmetry-breaking term induced by $H_{\rm em}$ in $\tilde{\mathcal{H}}_{0,0}$ without spin-orbit interaction (see Appendix A for details). This term gives rise to the photovoltaic anomalous Hall effect, as discussed in Sec. IV. In the following section, we derive the light-induced terms in the effective Hamiltonian within second-order perturbation theory.

We assume that, for perturbation theory, the energy scale of the incident light ($\hbar\Omega$) is larger than the width of the energy scale in Eq. (1). Then, the off-diagonal term is regarded as a perturbation for $\mathcal{H}_0$, and the effective Hamiltonian $\mathcal{H}_{\rm eff} = \tilde{\mathcal{H}}_{0,0}$ in the periodic steady state is given by

$$\mathcal{H}_{\rm eff} = \mathcal{H}_0 + \frac{e^2|A_{\rm L}|^2}{2m}\tau^z s^0 + \frac{[\mathcal{H}_{0,-1}, \mathcal{H}_{0,1}]}{\hbar\Omega} + \mathcal{O}(A_{\rm L}^4). \tag{6}$$

The first and second terms are derived from the diagonal term $\mathcal{H}_{0,0}$. The third term is the second-order correction due to the off-diagonal terms. Note that the second term and third term are newly added in the Hamiltonian. Below, we consider the details of these terms and their physical meanings, which are summarized in Table I.

TABLE I. Effects of circularly polarized light along the z, x, and y axes in a semimetal with a line node on the $k_z = 0$ plane. PAHE indicates the photovoltaic anomalous Hall effect.

Axis	Induced term	PAHE
z	$\delta m_0 \tau^z s^0$	0
x	$\delta m_0 \tau^z s^0$, $-\mathcal{L}_x k_y \tau^x s^0$	$\sigma_{yz}^{\rm AHE}$
y	$\delta m_0 \tau^z s^0$, $-\mathcal{L}_y k_x \tau^x s^0$	$\sigma_{xz}^{\rm AHE}$

A. Light propagation along the z axis

When light propagates along the z axis, $\boldsymbol{A}_{\rm L}$ is given by

$$\boldsymbol{A}_{\rm L} = A_{\rm L}(\cos\Omega t, \sigma^z_{\rm L}\sin\Omega t, 0), \tag{7}$$

where $A_{\rm L} \equiv iE_{\rm L}/\Omega$ and $E_{\rm L}$ are the magnitudes of the vector potential and the electric field of the light, respectively. The spin angular momentum of light, $\sigma^z_{\rm L} = \pm 1$, indicates the chirality of right-handed and left-handed circularly polarized light. Then, $[\mathcal{H}_{0,-1}, \mathcal{H}_{0,1}]$ vanishes and the effective Hamiltonian is given by

$$\mathcal{H}_{\rm eff} = \mathcal{H}_0 + \delta m_0 \tau^z s^0, \tag{8}$$

where

$$\delta m_0 = \frac{e^2 E_{\rm L}^2}{2m\Omega^2}. \tag{9}$$

Thus, there is no time-reversal-symmetry-breaking term in $\mathcal{H}_{\rm eff}$. We find that in Eq. (8) the induced term is proportional to $\tau^z s^0$ and its sign is always positive $\delta m_0 > 0$; therefore, this term plays a role in decreasing m_0 of Eq. (1) by δm_0. In other words, m_0 is renormalized into $\bar{m}_0$;

$$m_0 \to \bar{m}_0 = m_0 - \delta m_0, \tag{10}$$

which means that applying light along the z direction simply changes the radius of the line node, assuming δm_0 is smaller than m_0.

A line node may induce the quasi-topological response of the electric polarization P_z and the orbital magnetization M_z along the z direction, which are proportional to m_0[36]. This result implies that the values of P_z and M_z can be controlled through the application of circularly polarized light along the z direction. We also find that the changes of P_z and M_z are independent of the chirality of the incident light.

B. Light along the y axis

When the incident light propagates along the y axis, a new term, which breaks the time-reversal symmetry, is induced, in addition to the δm_0 term, as shown below. $\boldsymbol{A}_{\rm L}$ is represented by

$$\boldsymbol{A}_{\rm L} = A_{\rm L}(\sigma^z_{\rm L} \sin\Omega t, 0, \cos\Omega t). \tag{11}$$

The off-diagonal term $\mathcal{H}_{0,-1} (= \mathcal{H}^\dagger_{0,1})$ is given by

$$\mathcal{H}_{0,-1} = \frac{ieE_{\rm L}}{2\hbar\Omega}\begin{pmatrix} -\frac{\hbar^2}{m}[\sigma^z_{\rm L} i k_x + k_z] & iv \\ -iv & \frac{\hbar^2}{m}[\sigma^z_{\rm L} i k_x + k_z] \end{pmatrix}, \tag{12}$$

and the third term in Eq. (6) becomes

$$\frac{1}{\hbar\Omega}[\mathcal{H}_{0,-1}, \mathcal{H}_{0,1}] = -\frac{ve^2 E_{\rm L}^2}{m\hbar\Omega^3}\sigma^z_{\rm L} k_x \tau^x s^0. \tag{13}$$

The above term is represented in the form of $i\boldsymbol{\mathcal{E}} \times \boldsymbol{\mathcal{E}}^* = |\boldsymbol{\mathcal{E}}|^2 \sigma^z_{\rm L} \boldsymbol{q}$, which indicates the direction of the light propagation and the chirality of the incident polarized light, where $\boldsymbol{q}$ is the unit vector of the incident light and $\boldsymbol{\mathcal{E}}$ and $\boldsymbol{\mathcal{E}}^*$ are the complex vector of the electric field and its complex conjugate, respectively. When the light is along the y axis, the complex vector is given by $\boldsymbol{\mathcal{E}} = E_{\rm L}(i, 0, 1)/\sqrt{2}$. As a result, the effective Hamiltonian is obtained to be

$$\mathcal{H}_{\rm eff} = \mathcal{H}_0 + \delta m_0 \tau^z s^0 - \mathcal{L}_y k_x \tau^x s^0, \tag{14}$$

with

$$\mathcal{L}_{a=x,y,z} = \frac{ive^2}{m\hbar\Omega^3}(\boldsymbol{\mathcal{E}} \times \boldsymbol{\mathcal{E}}^*)_a. \tag{15}$$

Note that the light-induced term, $\mathcal{L}_y k_x \tau^x s^0$, in Eq. (14) indicates the interaction depending on the spin angular momentum of the light ($\sigma^z_{\rm L}$), the orbital degrees of freedom (τ^x), and the momentum $\boldsymbol{k}$. The magnitude of the coefficient $\mathcal{L}_y$ is proportional to both the laser intensity and Ω^{-3}. The sign of $\mathcal{L}_y$ denotes the chirality and the propagation direction of the light. It is also found that nonzero $\mathcal{L}_y$ is generated by nonzero v, which is corresponding to the velocity in the z direction in Eq. (2).

C. Light along the x axis

The effective Hamiltonian for the light along the x axis is derived by the $\pi/2$ rotation of that along the y axis. $\boldsymbol{A}_{\rm L}$ is represented by

$$\boldsymbol{A}_{\rm L} = A_{\rm L}(0, \cos\Omega t, \sigma^z_{\rm L} \sin\Omega t). \tag{16}$$

The off-diagonal terms, $\mathcal{H}_{0,-1}$ $(= \mathcal{H}^\dagger_{1,0})$ and $\frac{1}{\hbar\Omega}[\mathcal{H}_{0,-1}, \mathcal{H}_{0,1}]$, are found to be

$$\mathcal{H}_{0,-1} = \frac{ieE_{\rm L}}{2\hbar\Omega}\begin{pmatrix} -\frac{\hbar^2}{m}[k^y + i\sigma^z_{\rm L} k^z] & -\sigma^z_{\rm L} v \\ \sigma^z_{\rm L} v & \frac{\hbar^2}{m}[k^y + i\sigma^z_{\rm L} k^z] \end{pmatrix},$$
$$\frac{1}{\hbar\Omega}[\mathcal{H}_{0,-1}, \mathcal{H}_{0,1}] = -\mathcal{L}_x \tau^x s^0 k^y. \tag{17}$$

Therefore, the effective Hamiltonian in the Floquet state is given by

$$\mathcal{H}_{\rm eff}(\boldsymbol{k}) = \mathcal{H}_0 + \delta m_0 \tau^z s^0 - \mathcal{L}_x k_y \tau^x s^0.$$

Note that the third term denotes the coupling between τ^x and k_y.

IV. PHOTOVOLTAIC ANOMALOUS HALL EFFECT

Using the effective Hamiltonian in Eq. (14), we consider the photovoltaic anomalous Hall effect, which is a characteristic type of transport in the Floquet state in the presence of both incident circularly polarized light and an applied DC electric field. The direction of the incident light and the applied electric field are along the y direction and x direction, respectively, as illustrated in Fig. 1. Note that before applying the circularly polarized light, there is no anomalous Hall effect.

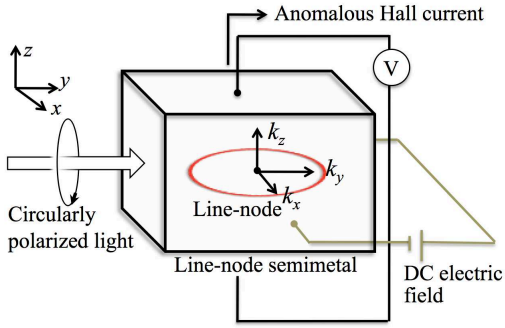

FIG. 1. (Color online) Schematic illustration of the setup for photovoltaic Hall effect measurement in a line-node semimetal. The incident light travels along the y direction and the DC electric field is applied along the x direction. The photovoltaic anomalous Hall current flows along the z direction.

The energy spectrum of Eq. (14) is found to be

$$E_{\pm}(\boldsymbol{k}) = -\epsilon_{\rm F} \pm \sqrt{\left(\frac{\hbar^2 k^2}{2m} - \bar{m}_0\right)^2 + v^2 k_z^2 + \mathcal{L}_y^2 k_x^2}, \quad (18)$$

which has Weyl points at $k_x = k_z = 0$ and $k_y = k_0$;

$$k_0 = \frac{\sqrt{2m\bar{m}_0}}{\hbar}. \quad (19)$$

The position of the Weyl point k_0 is slightly shifted by the change of $m_0 \to \bar{m}_0 = m_0 - \delta m_0$, as shown in Fig. 2. It is known that Weyl semimetals exhibit the anomalous Hall effect[42,43]; the present system under incident light also exhibit this effect, as explained below.

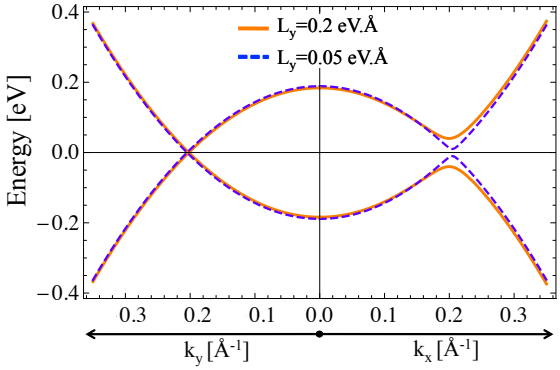

FIG. 2. (Color online) The energy dispersion of the line-node semimetal in the Floquet state at $k_z = 0$ and $\epsilon_{\rm F} = 0$ for two finite values of $\mathcal{L}_y$. Realistic parameters, i.e., $\hbar^2/(2m) = 4.5$ eV·Å^2, $v = 2.5$ eV·Å, and $m_0 = 0.184$ eV for Ca_3P_2, are used[15]. (Left panel) The k_y dependence of the energy dispersion of Eq. (18) with fixed $k_x = 0$. The position of the Weyl point is slightly shifted by the change $m_0 \to \bar{m}_0 = m_0 - \delta m_0$. (Right panel) The k_x dependence of Eq. (18) with fixed $k_y = 0$. A finite $\mathcal{L}_y$ value plays a role in opening the band gap, and the line-node vanishes.

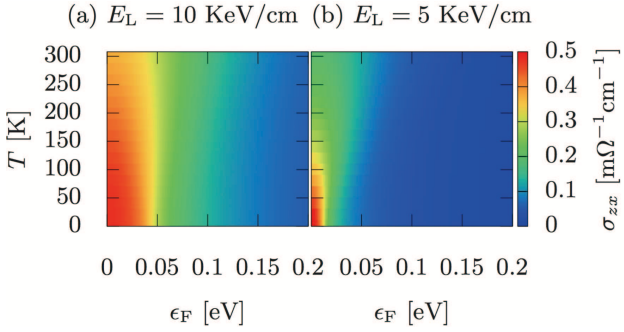

FIG. 3. (Color online) Anomalous Hall conductivity $\sigma_{zx}^{\rm AHE}$ for (a) $E_{\rm L} = 10$ KeV/cm and for (b) $E_{\rm L} = 5$ KeV/cm, as a function of the Fermi level $\epsilon_{\rm F}$ and the temperature T. This figure is based on realistic parameters for Ca_3P_2[15], which are the same those used in Fig. 2. The light frequency is set to $\Omega = 100/(2\pi)$ THz. The light-induced terms are evaluated as follows. (a) $\delta m_0 = 0.82$ meV, $\mathcal{L}_y = 0.2$ eV·Å for $E_{\rm L} = 10$ KeV/cm, and (b) $\delta m_0 = 0.21$ meV, $\mathcal{L}_y = 0.05$ eV·Å for $E_{\rm L} = 5$ KeV/cm, respectively. The two cases of (a) and (b) correspond to the solid and dashed lines in Fig. 2, respectively.

The Hall conductivity $\sigma_{zx}^{\rm AHE}$ is obtained using the Kubo formula:

$$\sigma_{zx}^{\rm AHE} = -i\hbar e^2 \int \frac{d^3k}{(2\pi)^3} \sum_{\alpha\neq\beta} [v_z(\boldsymbol{k})]_{\alpha\beta} [v_x(\boldsymbol{k})]_{\beta\alpha} \times \frac{f(\epsilon_{\rm F} + E_\alpha(\boldsymbol{k})) - f(\epsilon_{\rm F} - E_\beta(\boldsymbol{k}))}{[E_\alpha(\boldsymbol{k}) - E_\beta(\boldsymbol{k})]^2}, \quad (20)$$

where f is the Fermi distribution function and $v_i = (\partial H(\boldsymbol{k})/\partial k_i)/\hbar$ is the velocity matrix along the i-th axis. $\sigma_{zx}^{\rm AHE}$ is easily obtained for $\epsilon_{\rm F} = 0$ at zero temperature, $T = 0$. Because the system is a two-dimensional insulator for a fixed value of k_y (except for $k_y = k_0$), the two-dimensional Hall conductivity is quantized to $e^2/h \times \mathbb{Z}$. The Hall conductivity in the overall system is given by an integral, i.e.,

$$\sigma_{zx}^{\rm AHE}|_{\epsilon_{\rm F}=T=0} = 2 \times \frac{e^2}{h}\frac{k_0}{\pi}, \quad (21)$$

where the prefactor 2 is due to the spin degeneracy. This expression is the same as that in a Weyl semimetal in which the Weyl points are located at $k_y = \pm k_0$ and $k_x = k_z = 0$. Note that the above value depends only on the location of the Weyl points, irrespective of the induced time-reversal-symmetry-breaking term $\mathcal{L}_y$. For arbitrary $\epsilon_{\rm F}$ and T, $\sigma_{zx}^{\rm AHE}$ is numerically calculated, as shown in Fig. 3. For $\epsilon_{\rm F} \to 0$ and $T \to 0$, the value of $\sigma_{zx}^{\rm AHE} = 2e^2/h \times k_0/\pi = 0.5$ m$\Omega^{-1} \cdot$ cm^{-1} is reproduced for both cases shown in Figs. 3(a), 3(b), and the solid line in Fig. 4. The Hall conductivity is reduced by the effects of finite temperature and Fermi energy, except for finite Fermi energy in low temperatures.

The maximum of $\sigma_{zx}^{\rm AHE}$ (Eq. 21) has a large value for a large radius of the line node (m) and small $|E_{\rm L}/\Omega|$,

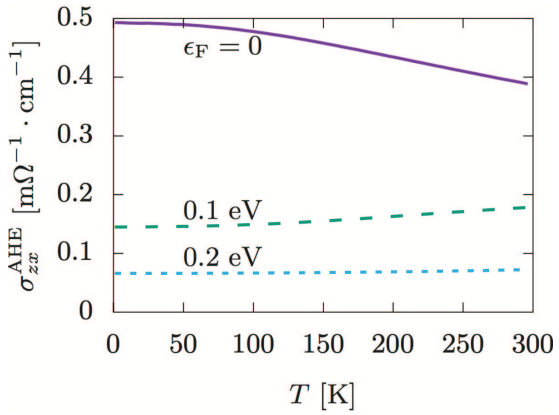

FIG. 4. (Color online) Temperature dependence of anomalous Hall conductivity for $\epsilon_{\rm F}=0$ eV (solid line), $\epsilon_{\rm F}=0.1$ eV (dashed line), and $\epsilon_{\rm F}=0.2$ eV (dotted line).

because of Eqs. (10) and (19). For finite $\epsilon_{\rm F}$ and T, on the other hand, $\mathcal{L}_y$ plays an important role: $\sigma_{zx}^{\rm AHE}$ is immediately suppressed when $\mathcal{L}_y$ is weak, because $\mathcal{L}_y$ is proportional to the magnitude of the light-induced gap, which is essential for ensuring the stability of the Hall conductivity for $\epsilon_{\rm F}\neq 0$ and $T\neq 0$.

Figure 4 shows the temperature dependence of $\sigma_{zx}^{\rm AHE}$ for three typical cases: (i) $\epsilon_{\rm F}=0$, for which the Fermi level is located only on the Weyl points; (ii) $\epsilon_{\rm F}=0.1$ eV, for which the carrier is moderately doped and the Fermi surface forms a torus; and (iii) $\epsilon_{\rm F}=0.2$, for which the carrier is sufficiently doped and a conventional spherical Fermi surface is realized. The Hall conductivity $\sigma_{zx}^{\rm AHE}$ monotonically and algebraically decreases as a function of T for $\epsilon_{\rm F}=0$ eV, whereas it slightly increases for finite Fermi energy ($\epsilon_{\rm F}=0.1$ eV and 0.2 eV) in the low-temperature regime and decreases to zero in the high-temperature limit (not shown in the figures).

V. DISCUSSION AND CONCLUSION

In this section, we will discuss an experimental realization of the circularly polarized light-induced effective Hamiltonian $\mathcal{H}_{\rm eff}$ and nonzero value of $\sigma_{zx}^{\rm AHE}$. The obtained result is verified when the energy scale of the incident light ($\hbar\Omega$) is much larger than that of the low-energy effective Hamiltonian $\mathcal{H}_0$, i.e., $\hbar\Omega\gg\epsilon_{\rm F}$. The light along the in-plane (xy) direction breaks the mirror-reflection symmetry that protects the line-node on the k_xk_y plane; therefore, the band gap opens, except at the Weyl points. As a result, the nonzero anomalous Hall current, which is a characteristic transport in the Floquet states, is driven by an applied DC electric field on the xy plane, where the line node is located and perpendicular to the light direction.

Fig. 3 shows that the magnitude of $\sigma_{zx}^{\rm AHE}$ is significantly reduced by having a finite value of $\epsilon_{\rm F}$, and that a large value of $\mathcal{L}_y$ is needed for the detection of a nonzero $\sigma_{zx}^{\rm AHE}$ in doped line-node semimetals. Recently, a method for generating a large electric field, i.e., over 1 MV/cm, at both infrared frequencies (72 THz)[44] and terahertz frequencies (1 THz)[45] has been reported. This light induces a giant orbital-momentum coupling $\mathcal{L}_y\approx 0.1$ eV.Å, which enables one to observe a large value of $\sigma_{zx}^{\rm AHE}$ in wide $\epsilon_{\rm F}$ and T regions [see Fig. 3(a)].

In a thin film of line-node semimetal, the Fermi level can be manipulated by applying a gate voltage. Thin films are also suitable for the irradiation of light, i.e., the light extends over the entire system when the thickness of the film is smaller than the wavelength of the light. For example, one can use a 1-μm (or thinner) film for visible light of high energy ($\hbar\Omega\sim 1$ eV $\gg\epsilon_{\rm F}$).

In addition, the anomalous Hall conductivity can be detected, even if the intensity of the light is weak, because $\sigma_{zx}^{\rm AHE}$ has a very large value for $\epsilon_{\rm F}\sim 0$, as shown in Fig. 3. Additionally, Eq. (21) shows that the anomalous Hall conductivity in the line-node semimetal is nearly independent of the laser intensity, and it is unlike that in Weyl semimetals: In Weyl semimetals with Floquet states, the anomalous Hall conductivity depends on the laser intensity, because the Weyl nodes are shifted by the circularly polarized light; this shift is proportional to the laser intensity[37–39]. In addition, we find that, unlike the light-induced effective Hamiltonian in Dirac/Weyl semimetals, this result is highly anisotropic regarding the direction of the incident light.

Finally, we consider applications of the photovoltaic anomalous Hall effect to optical and electrical devices. In the presence of a weak light, $\sigma_{zx}^{\rm AHE}(\epsilon_{\rm F})$ is roughly zero, except for $\epsilon_{\rm F}=0$, indicating that there are significant differences between $\sigma_{zx}^{\rm AHE}(\epsilon_{\rm F}\neq 0)$ and $\sigma_{zx}^{\rm AHE}(\epsilon_{\rm F}=0)$. The Fermi level, $\epsilon_{\rm F}$, is controlled by the on-off gate voltage in a thin film. Using the analogy to resistive random access memory or phase random access memory, the magnitude of the Hall conductivity $\sigma_{zx}^{\rm AHE}(\epsilon_{\rm F}\neq 0)$ and $\sigma_{zx}^{\rm AHE}(\epsilon_{\rm F}=0)$ can be regarded as "0" and "1" logic signals. This large difference in the Hall conductivity is applicable to optical and electrical memory devices or phototransistors. The basic mechanism could rely on the characteristic property of line-node semimetals. Additionally, we noted that the anomalous Hall effect is useful for the detection of the direction of light, because the nonzero value of $\sigma_{zx}^{\rm AHE}$ occurs when the light is along the mirror-symmetry-breaking direction of the line-node semimetal.

Note added.— During the preparation of the manuscript, we became aware of similar works by Z. Yan *et. al.*,[46], C.-K. Chan *et. al.*,[47], and A. Narayan[48], which discuss the transition from line-node semimetals to Weyl semimetals.

ACKNOWLEDGMENTS

The authors acknowledge fruitful discussions with Y. Tanaka. This work was supported by Grants-in-Aid for Core Research for Evolutional Science and Technology

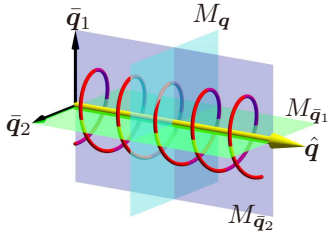

FIG. 5. Circularly polarized light along $\hat{\boldsymbol{q}}$ and mirrors.

(CREST) of the Japan Science and Technology Corporation, for Japan Society for the Promotion of Science (JSPS) Fellows, for Challenging Exploratory Research (Grant No.15K13498), and for Young Scientists (B, grant no. 16K17725).

Appendix A: Symmetry consideration for effective Hamiltonian induced by circularly polarized light

The form of the effective Hamiltonian in the Floquet state is determined by the symmetry consideration, as described below.

1. Symmetry of circularly polarized light

Circularly polarized light along the $\boldsymbol{q}$ direction is obtained from the vector potential of

$$\boldsymbol{A}_{\rm L} = R(\hat{\boldsymbol{q}})A_{\rm L}(\cos\Omega t, \sigma^z_{\rm L}\sin\Omega t, 0)^{\rm T},\ A_{\rm L}\in {\rm i}\mathbb{R}, \quad \text{(A1)}$$

where $R(\boldsymbol{q})\in {\rm SO}(3)$ is the rotational matrix that rotates $\hat{\boldsymbol{z}}$ into $\boldsymbol{q}$. The Hamiltonian describing the interaction between an electronic system and the light has the following form

$$H_{\rm em}(t) = -\boldsymbol{J}\cdot\boldsymbol{A}_{\rm L}, \quad \text{(A2)}$$

where $\boldsymbol{J}$ denotes the charge current of the system.

$H_{\rm em}(t)$ has mirror-reflection $M_{\boldsymbol{q}}$ symmetry perpendicular to $\boldsymbol{q}$, and rotational symmetry along $\boldsymbol{q}$. As a result, spatial-inversion symmetry is also retained. $\boldsymbol{J}$ is time-reversal odd. Time-reversal $\mathcal{T}$, on the other hand, reverses the chirality of the light, i.e., $H_{\rm em}(t)$ breaks time-reversal symmetry. The two mirrors, $M_{\bar{\boldsymbol{q}}_1}$ and $M_{\bar{\boldsymbol{q}}_2}$, are parallel to $\boldsymbol{q}$, as shown in Fig. 5; they also reverse the chirality. Therefore, $H_{\rm em}(t)$ is invariant for the composite operation, namely, so-called magnetic reflection, $M_{\bar{\boldsymbol{q}}_i}\mathcal{T}$;

$$(M_{\bar{\boldsymbol{q}}_i}\mathcal{T})^{-1}H_{\rm em}(t)(M_{\bar{\boldsymbol{q}}_i}\mathcal{T}) = H_{\rm em}(-t). \quad \text{(A3)}$$

Similarly, the magnetic-rotational $C(\pi\bar{\boldsymbol{q}}_i)\mathcal{T}$ symmetry along $\boldsymbol{q}$ holds.

In summary, $H_{\rm em}(t)$ is invariant under the following symmetry operations: $C(\theta\hat{\boldsymbol{q}})$, $M_{\boldsymbol{q}}$, I, $M_{\bar{\boldsymbol{q}}_i}\mathcal{T}$, $C(\pi\bar{\boldsymbol{q}}_i)\mathcal{T}$. For the realization of the photovoltaic Hall effect, the Floquet effective Hamiltonian must have a time-reversal-odd term of the A_{2g} representation or its compatible ones.

TABLE II. 16 matrices in the minimal theory.

	I	M_x	M_y	M_z	$\mathcal{T}$
$\tau^0 s^0$, $\tau^z s^0$	+	+	+	+	+
$\tau^0 s^x$, $\tau^z s^x$	+	+	−	−	−
$\tau^0 s^y$, $\tau^z s^y$	+	−	+	−	−
$\tau^0 s^z$, $\tau^z s^z$	+	−	−	+	−
$\tau^x s^0$	−	+	+	−	+
$\tau^x s^x$	−	+	−	+	−
$\tau^x s^y$	−	−	+	−	−
$\tau^x s^z$	−	−	−	−	−
$\tau^y s^0$	−	+	+	−	−
$\tau^y s^x$	−	+	−	+	+
$\tau^y s^y$	−	−	+	+	+
$\tau^y s^z$	−	−	−	−	+
k_x	−	−	+	+	−
k_y	−	+	−	+	−
k_z	−	+	+	−	−

2. Minimal model for a line-node semimetal

A minimal ($D_{\infty h}$) model hosting a line node consists of even-parity (i.e., $\tau^z=+1$) and odd-parity (i.e., $\tau^z=-1$) orbitals under mirror reflection with respect to the horizontal plane. The symmetry operations, spatial inversion I, and mirror reflection with respect to the $x_i=0$ plane M_i are represented by

$$I=\tau^z,\ M_x=s^x,\ M_y=s^y,\ M_z=\tau^z s^z. \quad \text{(A4)}$$

The 16 matrices $\tau^\mu\sigma^\nu$ in this theory are summarized in Table II.

A Hamiltonian for a line-node semimetal, which has an A_{1g} representation, is given by

$$H_0(\boldsymbol{k}) = c(\boldsymbol{k})\tau^0 s^0 + m(\boldsymbol{k})\tau^z s^0 + vk_z\tau^y s^0, \quad \text{(A5)}$$

where

$$c(\boldsymbol{k}) = c_0 + c_1 k_z^2 + c_2(k_x^2+k_y^2), \quad \text{(A6)}$$

$$m(\boldsymbol{k}) = m_0 + m_1 k_z^2 + m_2(k_x^2+k_y^2). \quad \text{(A7)}$$

In Eq. (1), for simplicity, the $c(\boldsymbol{k})$ term is ignored and $m_1=m_2$ is assumed.

In the following, we derive the effective Hamiltonian based on the symmetry consideration. The Floquet Hamiltonian shares the same symmetry as $H_0(\boldsymbol{k})+H_{\rm em}(t)$. $H_{\rm em}(t)$ renormalizes the parameters in $H_0(\boldsymbol{k})$ and yields new terms $\tilde{H}_{\rm em}(\boldsymbol{k})$. Here, we focus on the time-reversal-symmetry-breaking terms in $\tilde{H}_{\rm em}(\boldsymbol{k})$, which may trigger the photovoltaic anomalous Hall effect.

a. *Circularly polarized light along the z direction*

Symmetry of the system under circularly polarized light along the z direction is reduced to the point group

$\infty/mm'm'$ from ∞/mmm, where $'$ denotes the magnetic operation. The time-reversal-symmetry-breaking terms induced by the light belong to the time-reversal-odd A_{2g} representation of ∞/mmm;

$$\tilde{H}_{\rm em} = (a_{0z}\tau^0 + a_{zz}\tau^z)s^z + \lambda_y\tau^y(k_x s^x + k_y s^y) + a_{yz}k_z\tau^y s^z + \mathcal{O}(k^2). \quad \text{(A8)}$$

The light may induce many spin-dependent terms only when the system has a spin-orbit interaction.

b. Along the x direction

The symmetry of the system under circularly polarized light along the x direction becomes $m'mm'$ from ∞/mmm. The time-reversal-symmetry-breaking terms are the time-reversal-odd $E_{(2n-1)g}$ representation of ∞/mmm:

$$\tilde{H}_{\rm em} = (a_{0x}\tau^0 + a_{zx}\tau^z)s^x + \tau^y(a_{yz}k_x s^z + a_{yx}k_z s^x) + a_{x0}k_y\tau^x s^0 + \mathcal{O}(k^2). \quad \text{(A9)}$$

Similar to the previous case of light along the z direction, many spin-dependent terms may be induced in the presence of a spin-orbit interaction. Note that the last term arises, even in the absence of a spin-orbit interaction because it is independent of spin.

[1] M. Z. Hasan, and C. L. Kane, Rev. Mod. Phys. **82**, 3045 (2010).
[2] X.-L Qi, and S.-C. Zhang, Rev. Mod. Phys. **83**, 1057 (2011).
[3] A. A. Burkov, M. D. Hook, and L. Balents, Phys. Rev. B **84**, 235126 (2011).
[4] C.-K. Chiu, J. C. Y. Teo, A. P. Schnyder, and S. Ryu, arXiv:1505.03535.
[5] Z. K. Liu, B. Zhou, Y. Zhang, Z. J. Wang, H. M. Weng, D. Prabhakaran, S.-K. Mo, Z. X. Shen, Z. Fang, X. Dai, Z. Hussain, Y. L. Chen, Science **343**, 864 (2014).
[6] Z. K. Liu, J. Jiang, B. Zhou, Z. J. Wang, Y. Zhang, H. M. Weng, D. Prabhakaran, S-K. Mo, H. Peng, P. Dudin, T. Kim, M. Hoesch, Z. Fang, X. Dai, Z. X. Shen, D. L. Feng, Z. Hussain, and Y. L. Chen, Nat. Mater. **13**, 677 (2014).
[7] M. Neupane, S.-Y. Xu, R. Sankar, N. Alidoust, G. Bian, C. Liu, I. Belopolski, T.-Ro. Chang, H.-T. Jeng, H. Lin, A. Bansil, F. Chou, and M. Z. Hasan, Nat. Commun. **5**, 3786 (2014).
[8] X. Wan, A. M. Turner, A. Vishwanath, and S. Y. Savrasov, Phys. Rev. B **83**, 205101 (2011).
[9] S.-M. Huang, S.-Y. Xu, I. Belopolski, C.-C. Lee, G. Chang, B. Wang, N. Alidoust, G. Bian, M. Neupane, C. Zhang, S. Jia, A. Bansil, H. Lin, and M. Z. Hasan, Nat. Commun. **6**, 7373 (2015).
[10] H. Weng, C. Fang, Z. Fang, B. A. Bernevig, and X. Dai, Phys. Rev. X **5**, 011029 (2015).
[11] S.-Y. Xu, I. Belopolski, N. Alidoust, M. Neupane, C. Zhang, R. Sankar, S.-M. Huang, C.-C. Lee, G. Chang, B. Wang, G. Bian, H. Zheng, D. S. Sanchez, F. Chou, H. Lin, S. Jia, and M. Z. Hasan, Science **349**, 613 (2015).
[12] B. Q. Lv, H. M. Weng, B. B. Fu, X. P. Wang, H. Miao, J. Ma, P. Richard, X. C. Huang, L. X. Zhao, G. F. Chen, Z. Fang, X. Dai, T. Qian, and H. Ding, Phys. Rev. X **5**, 031013 (2015).
[13] S.-Y. Xu, N. Alidoust, I. Belopolski, Z. Yuan, G. Bian, T.-R. Chang, H. Zheng, V. N. Strocov, D. S. Sanchez, G. Chang, C. Zhang, D. Mou, Y. Wu, L. Huang, C.-C. Lee, S.-M. Huang, B. Wang, A. Bansil, H.-T. Jeng, T. Neupert, A. Kaminski, H. Lin, S. Jia, and M. Z. Hasan, Nat. Phys. **11**, 748 (2015).
[14] L. X. Yang, Z. K. Liu, Y. Sun, H. Peng, H. F. Yang, T. Zhang, B. Zhou, Y. Zhang, Y. F. Guo, M. Rahn, D. Prabhakaran, Z. Hussain, S.-K. Mo, C. Felser, B. Yan, and Y. L. Chen, Nat. Phys. **11**, 728 (2015).
[15] Y.-H. Chan, C.-K. Chiu, M. Y. Chou, and A. P. Schnyder, Phys. Rev. B **93**, 205132 (2016).
[16] C.-K. Chiu and A. P. Schnyder, Phys. Rev. B **90**, 205136 (2014).
[17] C. Fang, Y. Chen, H.-Y. Kee, and L. Fu, Phys. Rev. B **92**, 081201(R) (2015).
[18] M. N. Ali, Q. D. Gibson, T. Klimczuk, and R. J. Cava, Phys. Rev. B **89**, 020505 (2014).
[19] L. S. Xie, L. M. Schoop, E. M. Seibel, Q. D. Gibson, W. Xie, R. J. Cava, arXiv: 1504.01731.
[20] Y. Kim, B. J. Wieder, C. L. Kane, and A.M. Rappe, Phys. Rev. Lett. **115**, 036806 (2015).
[21] R. Yu, H. Weng, Z. Fang, X. Dai, and X. Hu, Phys. Rev. Lett. **115**, 036807 (2015).
[22] G. Bian, T.-R. Chang, H. Zheng, S. Velury, S.-Y. Xu, T. Neupert, C.-K. Chiu, D. S. Sanchez, I. Belopolski, N. Alidoust, P.-J. Chen, G. Chang, A. Bansil, H.-T. Jeng, H. Lin, and M. Z. Hasan, arXiv: 1508.07521.
[23] H. Weng, X. Dai, and Z. Fang, arXiv:1603.04744.
[24] H. Huang, J. Liu, D. Vanderbilt, and W. Duan, Phys. Rev. B **93**, 201114(R) (2016).
[25] K. Mullen, B. Uchoa, and D. T. Glatzhofer, Phys. Rev. Lett. **115**, 026403 (2015).
[26] G. Bian, T.-R. Chang, R. Sankar, S.-Y. Xu, H. Zheng, T. Neupert, C.-K. Chiu, S.-M. Huang, G. Chang, I. Belopolski, D. S.Sanchez, M. Neupane, N. Alidoust, C. Liu, B. Wang, C.-C. Lee, H.-T. Jeng, A. Bansil, F. Chou, H. Lin, and M. Z. Hasan, arXiv:1505.03069.
[27] L. M. Schoop, M. N. Ali, C. Straßer, V. Duppel, S. S. P. Parkin, B. V. Lotsch, and C. R. Ast, arXiv:1509.00861.
[28] L. S. Xie, L. M. Schoop, E. M. Seibel, Q. D. Gibson, W. Xie, and R. J. Cava, APL Mater. **3**, 083602 (2015).
[29] M. Neupane, I. Belopolski, M. M. Hosen, D. S. Sanchez, R. Sankar, M. Szlawska, S.-Y. Xu, K. Dimitri, N. Dhakal, P. Maldonado, P. M. Oppeneer, D. Kaczorowski, F. Chou, M. Z. Hasan, and T. Durakiewicz, Phys. Rev. B. **93**, 201104(R) (2016).

[30] Y. Wu, L.-L. Wang, E. Mun, D. D. Johnson, D. Mou, L. Huang, Y. Lee, S. L. Bud'ko, P. C. Canfield and A. Kaminski, Nat. Phys. **12**, 667 (2016).
[31] J. Hu, Z. Tang, J. Liu, X. Liu, Y. Zhu, D. Graf, Y. Shi, S. Che, C. N. Lau, J. Wei, and Z. Mao, arXiv:1604.06860.
[32] D. Takane, Z. Wang, S. Souma, K. Nakayama, C. X. Trang, T. Sato, T. Takahashi, Y. Ando arXiv:1606.07957.
[33] J.-W. Rhim and Y. B. Kim, Phys. Rev. B **92**, 045126 (2015).
[34] J.-W. Rhim and Y. B. Kim, New. J. Phys. **18**, 043010 (2016).
[35] Z. Yan, P.-W. Huang, and Z. Wang, Phys. Rev. B **93**, 085138 (2016).
[36] S. T. Ramamurthy and T. L. Hughes, arXiv:1508.01205.
[37] S. Ebihara, K. Fukushima, and T. Oka, Phys. Rev. B **93**, 155107 (2016).
[38] C. K. Chan, P. A. Lee, K. S. Burch, J. H. Han, and Y. Ran, Phys. Rev. Lett. **116**, 026805 (2016).
[39] K. Taguchi, T. Imaeda, M. Sato, and Y. Tanaka, Phys. Rev. B. **93**, 201202(R) (2016).
[40] T. Oka and H. Aoki, Phys. Rev. B **79**, 081406(R) (2009).
[41] H. Weng, Y. Liang, Q. Xu, R. Yu, Z. Fang, X. Dai, and Y. Kawazoe, Phys. Rev. B. **92**, 045108 (2015).
[42] K.-Y. Yang, Y.-M. Lu, and Y. Ran, Phys. Rev. B **84**, 075129 (2011).
[43] A. A. Burkov Phys. Rev. Lett. **113**, 187202 (2014).
[44] A. Sell, A. Leitenstorfer, and R. Huber, Opt. Lett. **33**, 2767 (2008).
[45] H. Hirori, A. Doi, F. Blanchard, and K. Tanaka, Appl. Phys. Lett. **98**, 091106 (2011).
[46] Z. Yan and Z. Wang, arXiv:1605.04404v2.
[47] C.-K. Chan, Y.-T. Oh, J. H. Han, and P. A. Lee, arXiv: 1605.05696v1.
[48] A. Narayan, arXiv: 1607.02503v1.